Journal of Medicinal Chemistry

Article

pubs.acs.org/jmc

Synthesis and Characterization of a Novel Gadolinium-Based Contrast Agent for Magnetic Resonance Imaging of Myelination

Luca Frullano,[†] Junqing Zhu,[†] Robert H. Miller,[‡] and Yanming Wang*[,†]

[†]Departments of Radiology, Chemistry, and Biomedical Engineering, Case Center for Imaging Research, Division of Radiopharmaceutical Science, Case Western Reserve University, 11100 Euclid Avenue, Cleveland, Ohio 44106, United States

[‡]Department of Neuroscience, Case Western Reserve University, 11100 Euclid Avenue, Cleveland, Ohio 44106, United States

Supporting Information

ABSTRACT: Myelin is a membrane system that fosters nervous impulse conduction in the vertebrate nervous system. Myelin sheath disruption is a common characteristic of several neurodegenerative diseases such as multiple sclerosis (MS) and various leukodystrophies. To date, the diagnosis of MS is obtained using a set of criteria in which MRI observations play a central role. However, because of the lack of specificity for myelin integrity, the use of MRI as the primary diagnostic tool has not yet been accepted. In order to improve MR specificity, we began developing MR probes targeted toward myelin. In this work we describe a new myelin-targeted MR contrast agent, Gd-DODAS, based on a stilbene binding moiety and demonstrate its ability to specifically bind to myelin in vitro and in vivo. We also present evidence that Gd-DODAS generates MR contrast in vivo in T_1-weighed images and in T_1 maps that correlates to the myelin content.

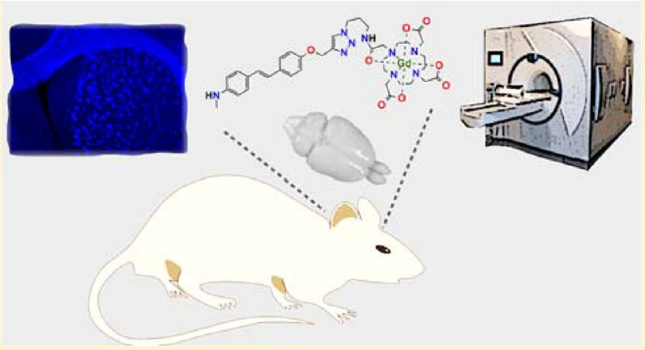

INTRODUCTION

Myelination is one of the most fundamental biological processes in the vertebrate nervous system.[1] The presence of myelin sheaths wrapped around axons provides the necessary electrical insulation for efficient nervous impulse conduction. Disruption of the compacted myelin sheath of axons is associated with a number of debilitating diseases such as multiple sclerosis (MS) and various leukodystrophies.[2,3] MS is the most common demyelinating disease, and it is characterized by demyelination in the central nervous system (CNS). MS affects an estimated 400 000 people in the U.S. and 2 million people worldwide.[4,5] The etiology of MS is complex and has both genetic and environmental factors contributing to the risk of disease. Risk factors include Epstein−Barr virus, vitamin D deficiency, and smoking.[6] MS is an inflammatory demyelinating disease that is considered by many to have an autoimmune origin. In the early phase of the disease, periods of active demyelination are followed by periodic and deteriorating remyelination. This phase is known as relapsing-remitting phase (RRMS). The RRMS phase is followed by a phase of continuous disease progression known as secondary progressive MS (SPMS). In some cases, during the transition from RRMS to SPMS, the continuous clinical deterioration is marked by active MS attacks (relapsing progressive multiple sclerosis, RPMS). Finally, about 10−20% of MS sufferers do not experience RRMS but present a continuous disease progression from the onset (primary progressive multiple sclerosis, PPMS).[7] In RRMS and in progressive MS, active tissue injury is associated with both demyelination and inflammation. The mechanism of myelin disruption has been extensively studied, and a wealth of experimental data have been reported.[8−11] Accordingly, various pathways underlying the process of demyelination have been proposed based on mitochondrial injury caused by oxidative stress or based on autoimmune response to autoantigens.

Over the past decade, magnetic resonance imaging (MRI) has played an important role in the diagnosis and disease management of MS.[12] Diagnosis of MS is normally guided by the revised McDonald criteria as recommended by the International Panel on the Diagnosis of Multiple Sclerosis.[13] In 2001, MRI was first incorporated into the criteria as an imaging tool to facilitate diagnosis and subtyping of MS. Since then, the McDonald criteria have been frequently revised, but they always included MRI as an indispensable tool to simplify diagnosis and provide a more accurate identification of the disease. Furthermore, tremendous efforts are being made to promote myelin repair in the brain as a new therapeutic strategy to restore neurological functions in the treatment of MS.[14] Development of myelin repair therapies must be accompanied by an imaging tool that can specifically and longitudinally monitor myelination. While MRI is very effective in detecting brain lesions, conventional MR techniques do not provide specific information on myelin pathology in the course

Received: October 3, 2012
Published: January 11, 2013

dx.doi.org/10.1021/jm301435z | J. Med. Chem. 2013, 56, 1629−1640

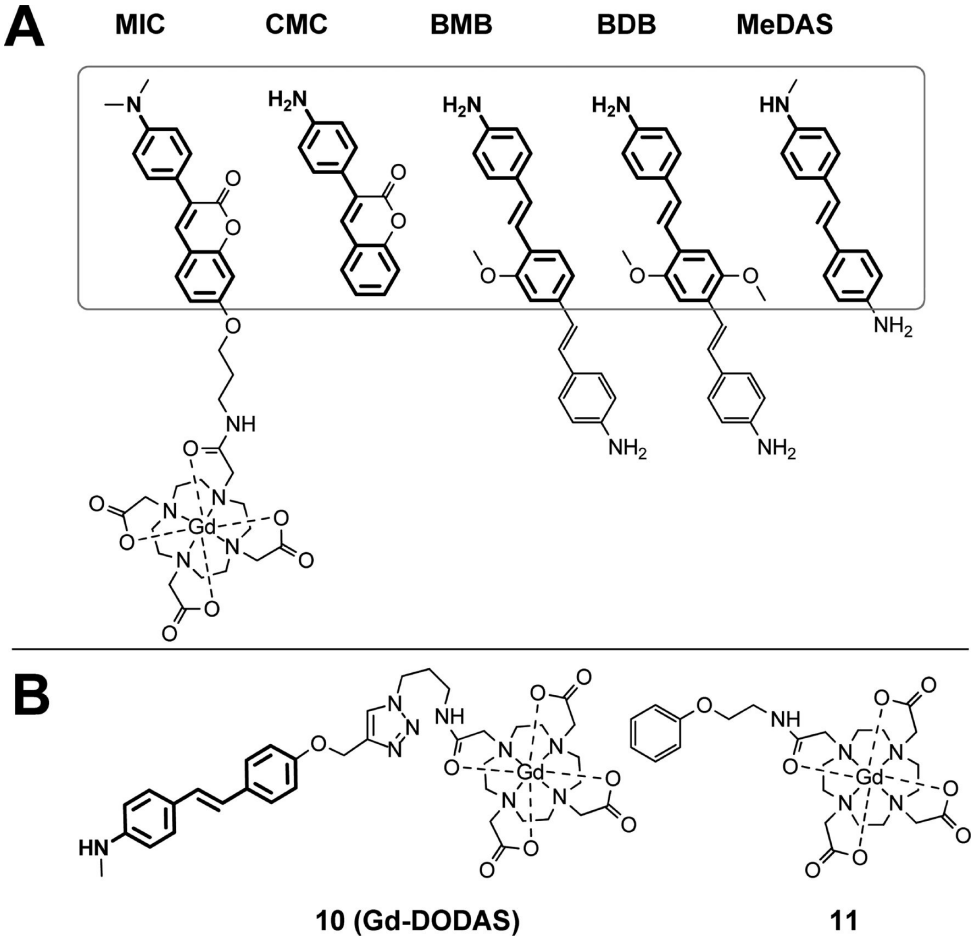

Figure 1. (A) Chemical structure of myelin-targeting probes previously identified by our group (MIC = gadolinium(III) [4,10-bis-carboxymethyl-7-({3-[3-(4-dimethylaminophenyl)-2-oxo-2*H*-chromen-7-yloxy]-propylcarbamoyl}methyl)-1,4,7,10-tetraazacyclododec-1-yl]acetate; CMC = 3-(4-aminophenyl)-2*H*-chromen-2-one; BMB = 4,4′-((1*E*,1′*E*)-(2-methoxy-1,4-phenylene)bis(ethene-2,1-diyl))dianiline; BDB = 4,4′-((1*E*,1′*E*)-(2,5-dimethoxy-1,4-phenylene)bis(ethene-2,1-diyl))dianiline; MeDAS = (*E*)-4-(4-aminostyryl)-*N*-methylaniline). In bold is highlighted a shared structural motif that is involved in binding with myelin. (B) Chemical structure of complexes that are discussed in this paper (Gd-DODAS, gadolinium (*E*)-2,2′,2″-(10-(2-((3-(4-((4-(4-(methylamino)styryl)phenoxy)methyl)-1*H*-1,2,3-triazol-1-yl)propyl)amino)-2-oxoethyl)-1,4,7,10-tetraazacyclododecane-1,4,7-triyl)triacetic acetate; compound **11**, gadolinium 2,2′,2″-(10-(2-oxo-2-((2-phenoxyethyl)amino)ethyl)-1,4,7,10-tetraazacyclododecane-1,4,7-triyl)triacetate).

of disease progression.[15,16] For example, lesions detected by T_2-weighed images are not directly related to demyelination or remyelination: they could also originate from an increased fraction of mobile water protons in regions where myelin is replaced with gliosis or from edema where myelin sheaths may remain intact. MS lesions can also be detected in T_1-weighed images, but they are less sensitive than T_2-weighed images and, likewise, do not correlate with myelin pathology of underlying tissues. Clinical contrast agents such as Gd-DTPA (DTPA = diethylenetriamine pentaacetic acid) are widely used for contrast-enhanced MR studies in MS patients. The use of these contrast agents is possible because of the fact that the blood−brain barrier (BBB) is often disrupted in MS patients. Thus, Gd-DTPA enhancement increases the reliability and sensitivity of detecting active lesions. However, none of the clinical contrast agents exhibit any affinity and specificity for myelin; instead, lesion enhancement by these agents is mainly indicative of disruption of the BBB. No information can be extracted from these images regarding myelin integrity in detected lesions. Recently gadofluorine, a fluorinated T_1 MR agent, has been reported. Gadofluorine binds to extracellular matrix proteins with high affinity and was found to detect brain lesions with high sensitivity in MR images.[17,18] Disruption of the BBB or blood to nerve barrier (BNB) allows the extravasation of gadofluorine, and binding to extracellular matrix protein provides lesion enhancement. However, gadofluorine enhancement does not reflect any changes in myelin integrity.

In order to improve the specificity of MR enhancement, we set out to develop myelin-specific contrast agents with optimal MR properties. Such myelin-targeting MR probes are crucial to establish the use of MRI for efficacy evaluation of novel myelin repair therapies currently under development. Over the past decade, our laboratory has developed a series of myelin-targeting molecular probes for multimodality imaging based on positron emission tomography (PET), MRI, and near-infrared (NIR).[19−25] Structure−activity relationship (SAR) studies of a library of compounds suggest a common structural motif that is important for binding to myelin (Figure 1A). On the basis of this knowledge, we explored the incorporation of some of these probes into the design of gadolinium-based contrast agents for MR studies of myelin pathology. We first developed gadolinium(III) [4,10-bis-carboxymethyl-7-({3-[3-(4-dimethylaminophenyl)-2-oxo-2*H*-chromen-7-yloxy]propylcarbamoyl}-

dx.doi.org/10.1021/jm301435z | *J. Med. Chem.* 2013, 56, 1629−1640

Scheme 1. Synthesis of Compound 10[a]

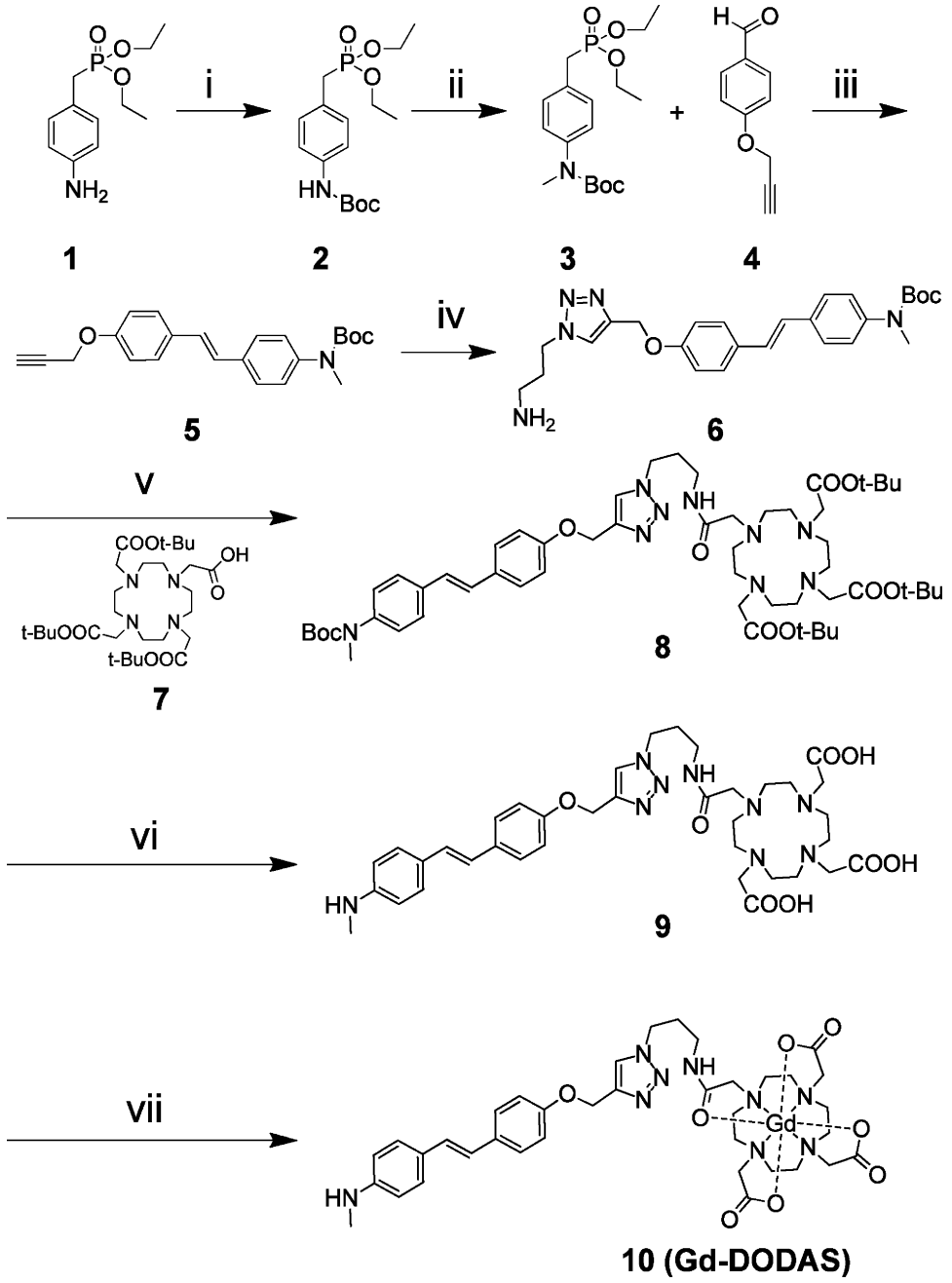

[a](i) Boc_2O, THF, 96%; (ii) MeI, NaH, THF, 94%; (iii) NaH, DMF, 83%; (iv) 3-azidopropan-1-amine, CuI, DIPEA, 54%; (v) HBTU, HOBT, DIPEA, DMF, 92%; (vi) TFA; (vii) $GdCl_3$, pH 5.5, 50% (over two steps).

methyl)-1,4,7,10-tetraazacyclododec-1-yl]acetate), a myelin-targeting MR agent termed MIC (Figure 1), which is based on a coumarin binding moiety, and demonstrated that MIC binds to myelin sheaths in vitro and in vivo and could be used to characterize myelin distribution based on T_{1w} MR imaging in murine models.[26,27] This demonstrated the validity of this strategy and that it is possible to integrate previously developed myelin-imaging agents into the design of MR contrast agents without negative impact on the myelin-binding properties. In order to increase the structural diversity of the pool of myelin targeted agents, we designed and synthesized a second type of myelin-targeted MR contrast agent bearing an aminostilbene moiety, Gd-DODAS (compound **10**, Figure 1B). The synthesis of **10**, along with biological evaluation of binding properties and MR relaxometric properties in vivo, is described in comparison with the previously developed MIC.

RESULTS

Synthesis. The myelin-targeting MR contrast agent **10** was prepared in seven steps from *p*-aminobenzyldiethyl phosphonate **1** (Scheme 1). The amino group was initially protected with Boc and subsequently methylated with methyl iodide to generate intermediate **3** in 90% yield over two steps. Intermediate **5**, carrying a terminal alkyne group, was prepared from Horner–Wadsworth–Emmons reaction of **3** and **4** in 83% yield. Copper(I)-catalyzed azide–alkyne cycloaddition

dx.doi.org/10.1021/jm301435z | J. Med. Chem. 2013, 56, 1629–1640

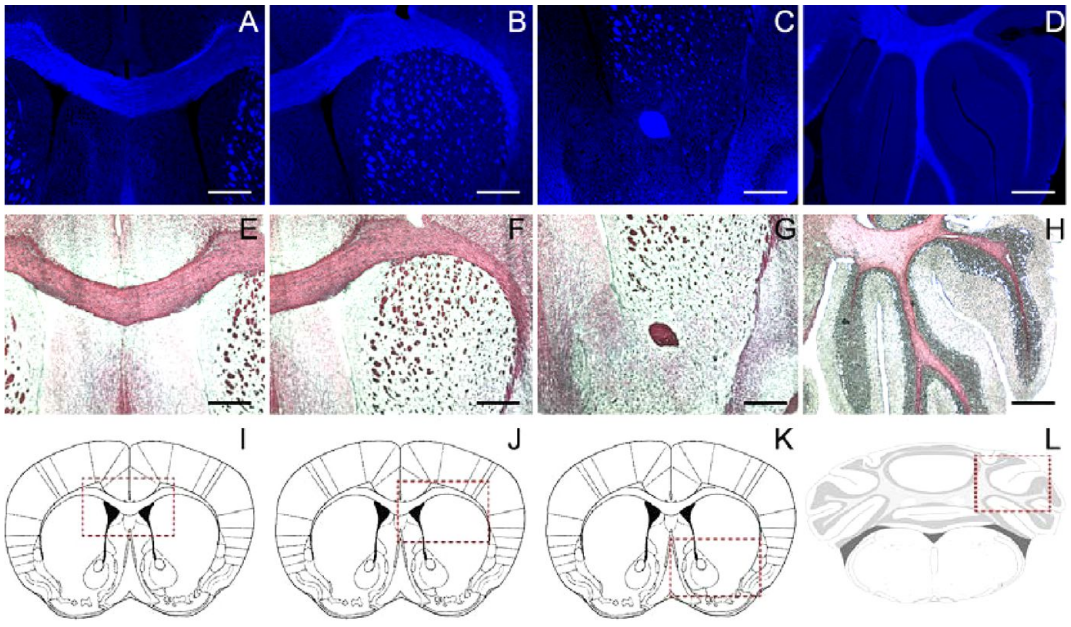

Figure 2. Chemical staining of representative frozen sections of wild-type mouse brain showing that **10** selectively stains various myelinated white matter regions in the brain such as corpus callosum, striatum, anterior commissure, and cerebellum (A–D, respectively). Gd-DODAS staining were correlated with Black-Gold II staining of adjacent sections (E–H). Atlas figures representing the stained regions are also shown (I–L).[30] Scale bar = 500 μm.

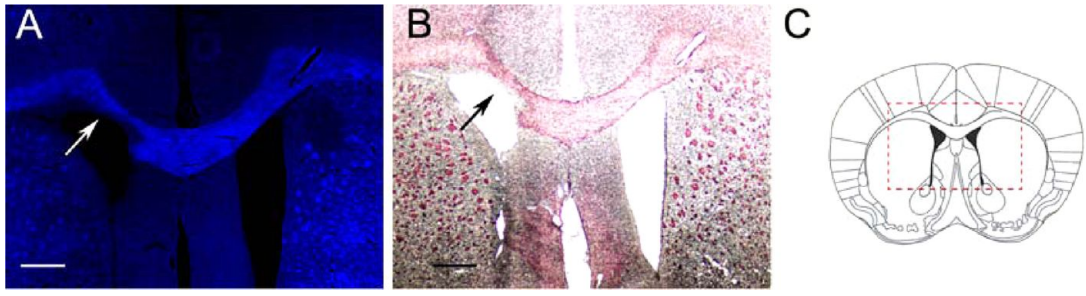

Figure 3. (A) Chemical staining with **10** of a brain section of LPC-treated rat. (B) The correspondence of compound **10** fluorescence with myelin distribution within the brain was confirmed by black Black-Gold II staining. The demyelinated lesion is indicated by the arrow. Scale bar = 500 μm. (C) Atlas figure shows the represented region.[31]

between intermediate **5** and 3-azidopropylamine was used to prepare compound **6**, which was subsequently coupled to tris-*t*-Bu protected DOTA to give the protected ligand **8** in 50% yield over two steps. Deprotection of the *t*-Bu groups in neat TFA and metalation with $GdCl_3$ afforded **10** in 50% yield over the last two steps with a 19% overall yield.

In Vitro Chemical Staining. The absorption spectrum of compound **10** shows a single intense long wavelength band with a maximum of absorbance at 341 nm. The fluorescent spectrum of **10** in water is similar to those of other *p*-aminostilbenes with a fluorescence maximum at 443 nm and a Stokes shift of 6848 cm^{-1}.[28] The emission spectrum does not show any vibrational structure.

Because of the fluorescent nature of **10**, its myelin binding properties were first investigated by analyzing the fluorescent staining pattern on freshly frozen tissue sections of 2-month-old Swiss–Webster R/J mouse brains. Axial sections of the whole mouse brain close to the bregma were used to examine the myelin-binding properties of **10** in both myelin-deficient gray and myelin-rich white matter regions. Axial sections were used to examine staining in the cerebellum.

As shown in Figure 2, **10** preferentially stains myelin-rich white matter regions such as the corpus callosum (Figure 2A), the external capsule (Figure 2B), striatum (Figure 2B), the anterior commissure (Figure 2C), and the cerebellum (Figure 2D). Myelin distribution was covalidated by chemical staining with Black-Gold II, a commonly used myelin stain, on adjacent sections.[29] As displayed in Figure 2E–H, chemical staining with Black-Gold II and with compound **10** showed an identical pattern, which suggests that compound **10** binds to myelin with high specificity.

Compound **10** was also able to detect demyelinated lesions in vitro in a rat model of focal demyelination. For this purpose, Sprague–Dawley rats were treated with lysolecithin (LPC), a neurotoxin that induces demyelination at the site of injection. As shown in Figure 3, the LPC-induced lesions in the corpus callosum can be readily detected by fluorescent staining with **10** as characterized by decreased fluorescence intensity. The same demyelinated lesion was confirmed by Black-Gold II staining of myelin in an adjacent brain tissue section.

The binding specificity and sensitivity of **10** for myelin was then further evaluated using a hypermyelinated *Plp*-Akt-DD transgenic mouse model.[32,33] Chemical staining with com-

dx.doi.org/10.1021/jm301435z | *J. Med. Chem.* 2013, 56, 1629–1640

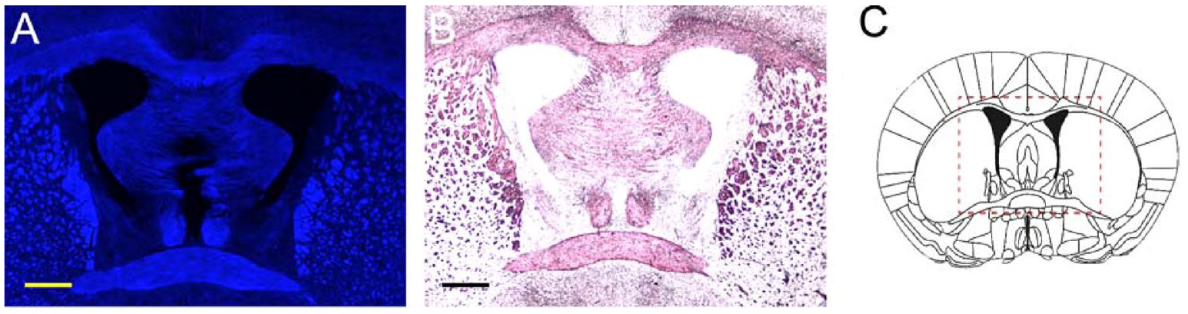

Figure 4. (A) Chemical staining with compound **10** of a brain section of a hypermyelinated *Plp*-Akt-DD D transgenic mouse. (B) The correspondence of compound **10** fluorescence with myelin distribution within the brain was confirmed by Black-Gold II staining. Scale bar = 250 μm. (C) Atlas figure shows the represented region.[30]

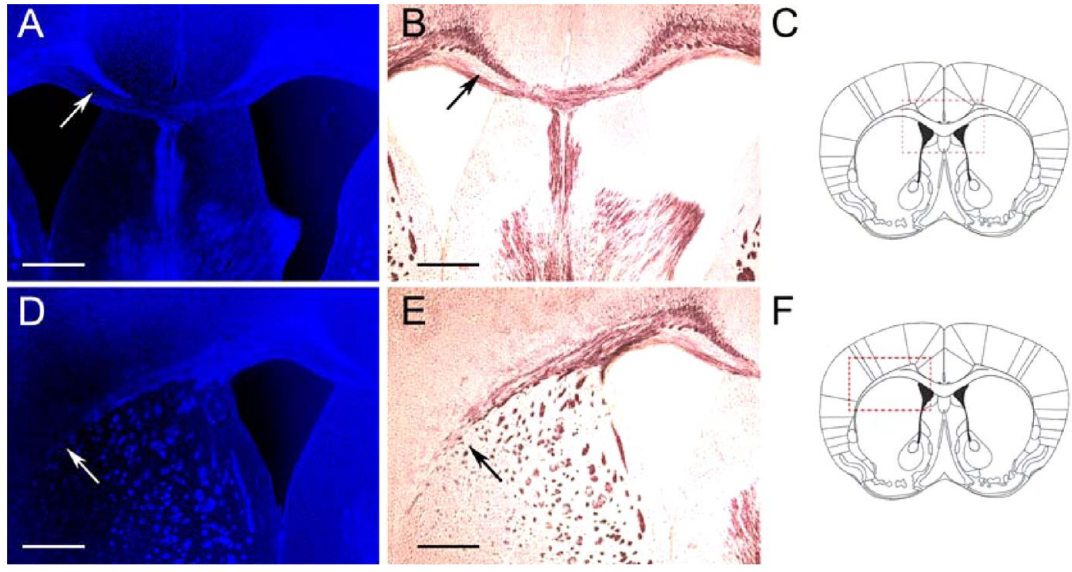

Figure 5. Chemical staining with compound **10** of a brain section of a cuprizone mouse model showing demyelinated lesions (arrows) in the corpus callosum (A) and external capsule (B). Demyelination was confirmed by Black-Gold II staining (D, E). Atlas figures show the represented regions (C, F).[30]

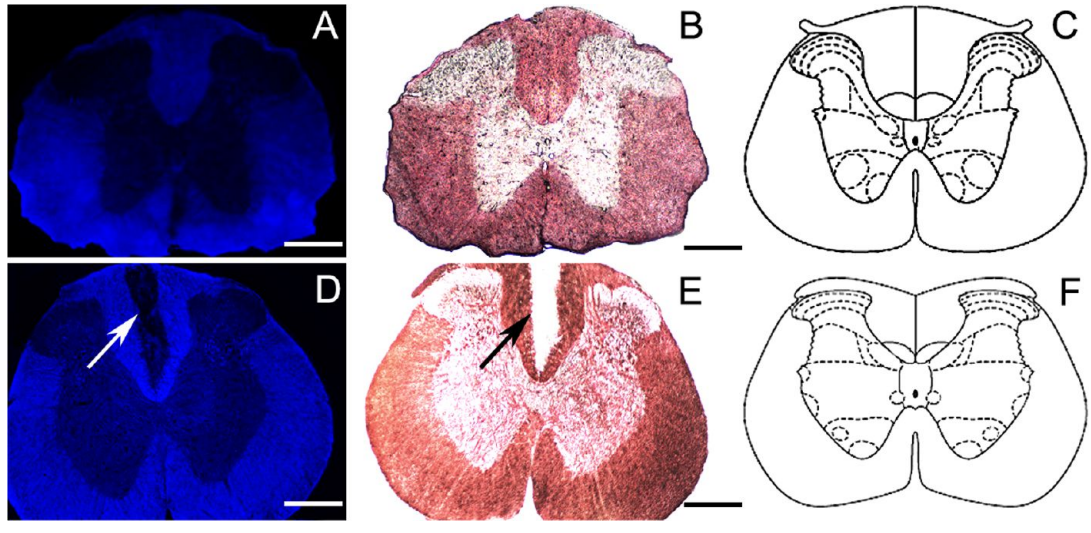

Figure 6. Chemical staining with compound **10** of an axial spinal cord section of a wild type mouse (A) and Black-Gold II staining of an adjacent section (B). A large demyelinated lesion (arrow) can be detected in a spinal cord section of an LPC-induced mouse model of demyelination (D). The demyelinated lesion was confirmed by Black-Gold II staining of an adjacent section (E). Spinal cord diagrams show the represented regions (C, F).

dx.doi.org/10.1021/jm301435z | *J. Med. Chem.* 2013, 56, 1629−1640

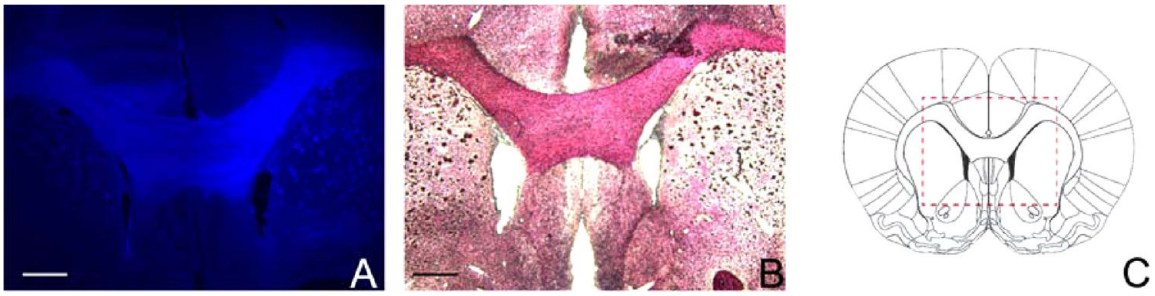

Figure 7. (A) In situ fluorescent microscopy of a brain tissue section following in vivo contrast enhanced MR imaging. (B) Bright field microscopy Black-Gold II myelin staining of an adjacent section. Scale bar = 500 μm. (C) Atlas figure shows the represented region.[31]

pound **10** of hypermyelinated *Plp*-Akt-DD transgenic mice frozen brain sections reveals the hypertrophic corpus callosum characteristic of this model (Figure 4). The same staining pattern is also observed by Black-Gold II staining using adjacent brain tissue sections.

In order to prove that compound **10** is able to identify demyelinated lesions in an animal model of the MS disease, frozen brain sections of cuprizone mouse brains were chemically stained with compound **10**. In this model of toxic demyelination, mice are fed with the copper chelator cuprizone, which induces oligodendrocyte cell death and consequently demyelination. Sections stained with compound **10** revealed large demyelinated lesions in the corpus callosum and the external capsule. The demyelinated nature of these lesions was confirmed by Black-Gold II staining (Figure 5).

We investigated the capability of compound **10** to bind myelin other than in the brain white matter. For this purpose spinal cord sections of wild type mice were chemically stained with compound **10**. The staining pattern observed correctly reflects the distribution of white matter in the spinal cord as covalidated by Black-Gold II staining of adjacent sections (Figure 6A,B). Furthermore, we demonstrated that compound **10**, similar to what was observed in the brain, is able to detect demyelinated lesions induced by LPC injection in the spinal cord (Figure 6D,E).

In Situ Chemical Staining. In situ staining of compound **10** was studied following intraventricular infusion in wild-type Sprague–Dawley rats. The rats were euthanized and perfused with 4% paraformaldehyde to remove the blood. The brains were extracted and dissected to prepare frozen axial sections. Fluorescent microscopy shows that **10** is selectively localized in myelinated regions such as corpus callosum and striatum (Figure 7). Adjacent sections were then subjected to Black-Gold II staining for myelin. As shown in Figure 6, the pattern of compound **10** staining (blue) is consistent with the pattern of Black-Gold II staining. These data suggest that **10** can selectively label myelin fibers in situ and potentially be used to monitor myelin changes in vivo.

Relaxometric Properties. The relaxometric properties of **10** were measured at 0.47 T (40 °C), 1.41 T (40 °C), and 9.4 T (21 °C), three magnetic field strengths commonly used in clinical and preclinical studies. Compound **10** relaxivity is dependent upon concentration (Figure 8). At high concentrations a sharp increase in relaxivity is observed at the two lower magnetic fields. At 9.4 T, the relaxivity at higher concentration is almost identical to the low concentration relaxivity. The high dilution relaxivities of **10** at the measured fields in comparison with previously reported MIC and other clinical contrast agents are reported in Table 1.

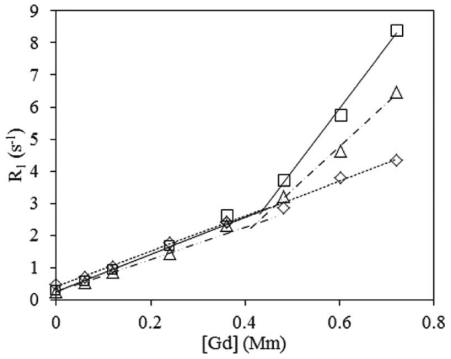

Figure 8. Dependence of the relaxation rate of PBS buffered solutions (pH 7.4) of **10** upon Gd concentration at 0.47 T (40 °C, squares), 1.41 T (40 °C, triangles), and 9.4 T (21 °C, diamonds).

Table 1. Longitudinal Relaxivity of Compound 10 Compared to MIC and the Clinically Approved MR Contrast Agents GdDTPA and GdDOTA

	r_1 (s^{-1} mM^{-1})			
magnetic field (T)	**10**	MIC	GdDTPA	GdDOTA
0.47	5.8 ± 0.2[a]	5.8 ± 0.2[a]	3.4 ± 0.2[34,a]	3.4 ± 0.2[34,a]
1.41	5.1 ± 0.2[a]	5.1 ± 0.1[a]	3.3 ± 0.2[34,c]	2.9 ± 0.2[34,c]
9.4	5.5 ± 0.3[b]	5.2 ± 0.1[b]	3.9[35,d]	4.1[35,d]

[a]40 °C. [b]21 °C. [c]1.5 T, 37 °C. [d]25 °C.

In Vivo MR Imaging. Similar to other Gd-based contrast agents, **10** is a hydrophilic compound that is not permeable across the BBB. For this reason, we evaluated compound **10** brain biodistribution after intracerebroventricular infusion to bypass the BBB. Sprague–Dawley rats were anesthetized, and **10** (10 μL, 70 nmol) was administered via stereotaxic injection to the lateral ventricles (LV). The animals were imaged twice using a spin–echo multiple TR saturation recovery method 5 and 24 h after injection. As shown in Figure 9A, compound **10** induced a dramatic shortening of T_1 localized in correspondence of the corpus callosum. T_1 shortening was clearly visible at a dose of 70 nmol (~3.2 mg/kg) and persisted at least for 24 h after infusion (data not shown). In contrast, brain T_1 maps of untreated rats show little contrast between highly myelinated white matter and less myelinated gray matter regions (Figure 9B). T_1 maps of the rat brain infused with compound **11** (10 μL, 70 nmol), acquired 5 h after infusion, also lacked contrast between the white matter and gray matter, suggesting that compound **11**, which contains only part of the pharmacophore responsible for myelin binding, is not retained in highly myelinated regions of the brain and produces a uniform

dx.doi.org/10.1021/jm301435z | J. Med. Chem. 2013, 56, 1629–1640

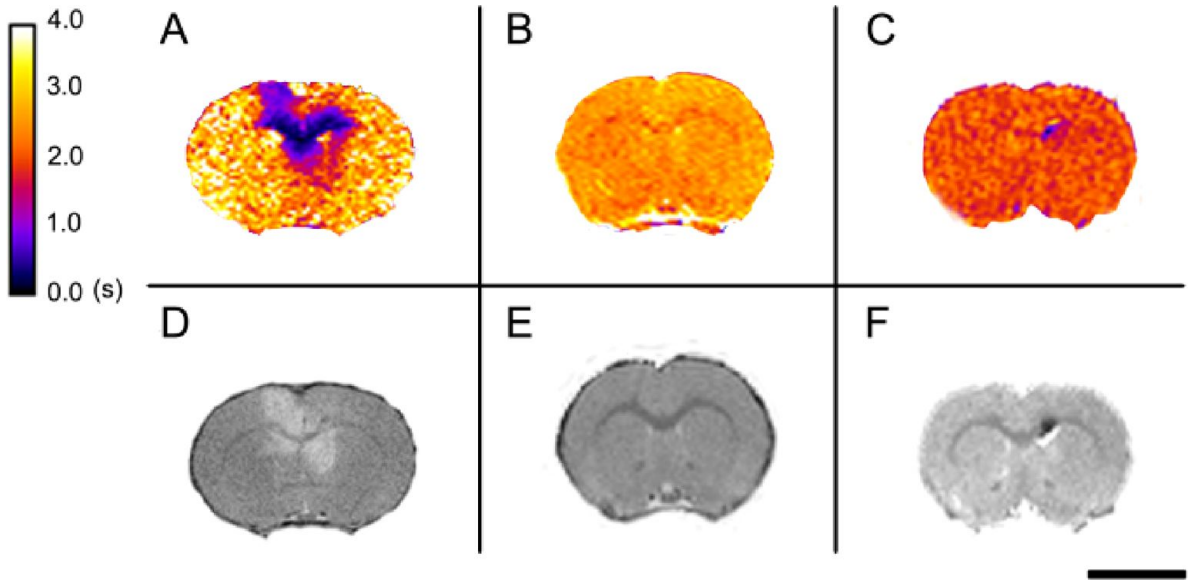

Figure 9. MR T_1 maps (spin−echo multiple TR saturation recovery, TE = 6.99 ms, TR = 385−12500 ms, spatial resolution = 0.195 × 0.195 mm/pixel, matrix size = 256 × 256, 30 slices, slice thickness = 0.5 mm, 1 average) of a (A) Sprague−Dawley rat brain 5 h after compound **10** injection, (B) Sprague−Dawley rat brain without infusion of contrast agent, (C) Sprague−Dawley rat brain after injection of compound **11** and corresponding anatomical images (D−F).

shortening of the longitudinal relaxation time throughout the brain (Figure 9C).

DISCUSSION

The inability of conventional MR to probe myelination status in the CNS and PNS prompted us to prepare MR contrast agents that could selectively interact with myelin sheaths. The design of the proposed agent is based on the structure of myelin probes for PET imaging that were previously identified in our group. SAR studies on a library of compounds revealed a common structural motif that is involved in binding with myelin (Figure 1A). These previously identified myelin probes, while sharing a common structural motif, can be categorized into coumarin and stilbene derivatives. We have recently reported the preparation and the myelin binding and MR properties of MIC, a myelin targeted MR agent derived from coumarin. In order to establish if myelin-targeted probes based on a stilbene core are also amenable to be functionalized with an MR reporter, we synthesized and characterized a novel myelin-targeting agent derived from an aminostilbene moiety conjugated with a DOTA monoamide gadolinium(III) complex. Compound **10** was synthesized in seven steps with an overall yield of ∼19%.

Gd(III) ions, because of their high magnetic moment and long electron relaxation time, are able to efficiently shorten the longitudinal or transversal relaxation rate (R_1 and R_2) of the solvent water protons. The effectiveness with which a paramagnetic agent is able to shorten the relaxation rate of solvent water protons is given by a parameter called relaxivity (r_i; i = 1, 2) which represents the increase in relaxation rate of a water solution occurring after the addition of the agent, normalized to a concentration of 1 mM (eq 1).

$$R_i = \frac{1}{T_i} = r_i[\mathrm{Gd}] + R_i^{\mathrm{solv}}; \quad i = 1, 2 \tag{1}$$

Here T_i is the longitudinal or transversal relaxation time of the solution, r_i is the relaxivity, and R_i^{solv} is the relaxation rate of the solvent. Relaxivity is not a constant but depends on a number of external parameters, such as the applied magnetic field strength and temperature, as well as molecular parameters including the number of coordinated water molecule(s) (q), the mean residence time (τ_M) of the coordinated water molecule(s), and the reorientational correlation time (τ_R). The relaxivity of small Gd complexes such as compound **10** is strongly influenced by the reorientational correlation time especially at magnetic fields lower than 1.5 T.

At 0.47 and 1.41 T (40 °C), the low concentration relaxivity of **10** is nearly identical to the relaxivity of MIC and about 1.5−1.7 times higher than that of commercial MR contrast agents such as GdDOTA or GdDTPA. Unlike MIC, compound **10** tends to aggregate in solution at concentrations above ∼0.4 mM, which is apparent from the increase in relaxivity observed at high concentration. The higher relaxivity observed under these conditions is a reflection of the increased rotational correlation time of the aggregated complex. At 9.4 T, the increase in relaxivity is less pronounced, since the influence of the rotational correlation time upon the relaxivity becomes less important.[36] An increase in relaxivity can also be expected upon binding of compound **10** to myelin, provided that the metal center retains access to bulk water and that the bound water exchange rate is not significantly reduced.

Compound **10** is fluorescent, and therefore, it is possible to investigate its myelin-binding properties using fluorescent microscopy. For this purpose the ability of **10** to selectively bind myelin was investigated by chemical staining of wild type mouse brain sections. As shown in Figure 2, the fluorescence originating from **10** is more intense in highly myelinated white matter brain regions such as the corpus callosum, the external capsule, the caudate putamen, and the anterior commissure and in the cerebellar arbor vitae. The colocalization of compound **10** with the myelin distribution in the brain was confirmed by chemical staining with Black-Gold II, a commonly used myelin stain. The ability of **10** to detect and identify areas of decreased or increased myelination was tested by in vitro histochemistry of murine animal models of abnormal myelination. Chemical

dx.doi.org/10.1021/jm301435z | J. Med. Chem. 2013, 56, 1629−1640

staining with compound **10** of brain sections of an LPC rat model of demyelination (Figure 3) demonstrates that compound **10** can be used to identify focal demyelinated lesions. Decreased myelination was also easily detected in the corpus callosum and external capsule of a cuprizone mouse model of demyelinating disease (Figure 5). Furthermore, histochemical staining of AKT mouse brain with compound **10** showed an increased fluorescence in highly myelinated white matter that correlates well to the enhanced myelination that is characteristic of this kind of animal model (Figure 4).

Myelin is a complex blend of proteins and lipids, and its composition changes not only between the CNS and PNS but also within the CNS.[1] In order to test if compound **10** retains its binding ability to myelin fibers outside the brain, we stained axial sections of a wild type spinal cord with compound **10** (Figure 6). The staining pattern observed for compound **10** reflects the myelin distribution within the spinal cord. Moreover, compound **10** could detect LPC-induced demyelinated lesion in the spinal cord of a wild type mouse similar to what was observed for brain lesions.

Once established that compound **10** is able to selectively bind myelin sheaths in vitro, its ability to bind myelin sheaths in vivo was tested by measuring its distribution in the brain of live animals by magnetic resonance imaging relaxometry. Compound **10** is a hydrophilic, highly water-soluble gadolinium complex with a molecular weight (904 Da) that exceeds 500 Da, a value that is usually recognized as the upper limit for BBB permeability by passive diffusion. Thus, like other clinical contrast agents, compound **10** is not permeable across the BBB. It is important to note that in MS the BBB is normally disrupted in correspondence of new or reactivated lesions. Therefore, compound **10** can be expected to cross the compromised BBB similar to GdDTPA. In the present study, we examined the distribution of **10** in the brain of wild type rats with an intact BBB. In order to bypass the BBB, compound **10** was administered by intracerebroventricular infusion. T_1 maps generated 5 h postinfusion show that compound **10** accumulates preferentially in the highly myelinated genus of the corpus callosum. The diffusion from the site of injection is slow, and the contrast pattern in T_1 maps acquired 24 h postinjection remains unchanged (data not shown). The contrast pattern generated by compound **10** was compared with the pattern generated by compound **11**. Compound **11** is characterized by the same coordination cage as compound **10** modified with a hydrophobic moiety. T_1 maps obtained 5 h postinfusion show that compound **11** does not accumulate in highly myelinated region and produces a uniform decrease of the longitudinal relaxation time throughout the entire brain (Figure 9C).

CONCLUSION

There is an urgent and unmet need to improve the sensitivity of MR techniques toward myelin changes in the nervous system. Such improvements will facilitate the early diagnosis of neurodegenerative diseases such as MS, provide a powerful tool to monitor response to current and new therapies, and assist in drug development.

A number of myelin-targeting probes for PET and optical imaging have been previously developed in our group. Optical imaging is an effective tool for preclinical drug development; however, it lacks deep tissue penetration, while PET, despite having a superb sensitivity, is characterized by a low resolution and lack of anatomical information. MRI, on the other hand, can provide deep tissue penetration, high resolution, and an excellent soft tissue contrast. For this reason, we decided to modify our previously developed probes for MR imaging. We recently reported MIC, a Gd complex containing a coumarin binding moiety, as the first myelin-targeting MR contrast agent. In this work we describe the synthesis, relaxometric characterization, and myelin binding properties of compound **10**, the first MR myelin-targeting agent based on a stilbene binding moiety. Compound **10** binding to myelin was demonstrated both in vitro and in situ by fluorescent microscopy and in vivo by T_{1w} MR imaging. The fact that both myelin-targeted coumarin and stilbene probes can be successfully modified and functionalized with MR reporter while retaining their targeting specificity suggests that it is possible to create structurally diverse libraries of myelin-targeted MR probes by modifying the lanthanide-chelating unit. Like all the other hydrophilic MR probes, BBB permeability of **10** remains a challenge. In this work we exploited intracerebroventricular infusion to bypass the BBB. A number of methodologies have been reported in the literature to shuttle hydrophilic compounds across the BBB, and we are currently exploring the application of some of these techniques to deliver these agents. The utility of these probes, however, is not entirely dependent on their ability to cross the intact BBB. In neurodegenerative diseases such as MS, the BBB is transiently open in active lesions, and this is already exploited clinically for GdDTPA-enhanced MR imaging. For this reason, we believe that the development of myelin-targeting MR probes can prove to be an extremely useful tool for neuroimaging.

EXPERIMENTAL SECTION

Materials and Methods. All chemicals, unless otherwise stated, were purchased from commercial sources and used without further purification. L-α-Lysophosphatidylcholine from egg yolk was purchased from Sigma-Aldrich. All NMR spectra were acquired on an Inova 400 NMR system (Varian) equipped with a 5 mm broadband probe. Analytical HPLC was performed on an Agilent 1100 series system equipped with a dual channel UV/vis detector using a Phenomenex 5 μm C18(2) 100A (250 mm × 4.56 mm, 5 μm) column (4.6 mm × 250 mm); eluent A, H_2O/0.1% TFA; B, MeOH/0.1% TFA; elution, 10% B 3 min, 10% B to 100% B in 15 min; flow rate 1 mL/min. The purity of tested compounds as determined by analytical HPLC was >95%. ESI mass spectra were acquired on a Finnigan LCQ Deca. pH was measured using a PHM210 standard pH meter (Radiometer Analytical) connected to a sympHony pH glass electrode (VWR). UV absorption was measured on a Cary 50 Bio spectrophotometer using a standard 1 cm × 1 cm quartz cuvette. Fluorescence was measured with a Cary Eclipse spectrophotofluorimeter using a standard 1 cm × 1 cm quartz cuvette.

***tert*-Butyl (4-((Diethoxyphosphoryl)methyl)phenyl)-carbamate (2).** To a 100 mL round-bottom flask fitted with a magnetic stir bar were added diethyl 4-aminobenzylphosphonate (**1**, 2.500 g, 10.28 mmol), di-*tert*-butyl dicarbonate (2.240 g, 10.27 mmol), THF (15 mL), and water (6.0 mL). The mixture was stirred at room temperature overnight. THF was removed in vacuo, and the resulting residue was diluted with water and extracted with EtOAC three times. The organic layers were combined and washed twice with water and once with brine. The organic layer was dried over $MgSO_4$, filtered, and concentrated in vacuum. The resulting white solid (3.393 g, 96%) was used without further purification. ^{1}H NMR ($CDCl_3$, 400 MHz) δ: 1.22 (6H, td, $^3J_{H,H}$ = 6.8 Hz, $^4J_{H,P}$ = 0.4 Hz, CH_2CH_3), 1.49 (9H, s, CCH_3), 3.07 (2H, d, $^2J_{H,P}$ = 21.2 Hz, PCH_2), 3.91−4.04 (4H, m, OCH_2), 6.87 (1H, br s, N*H*), 7.17 (2H, m, Ar*H*), 7.30 (2H, br d, J = 8.4 Hz, Ar*H*). ^{13}C NMR ($CDCl_3$, 100 MHz) δ: 16.3 (CH_2CH_3), 28.8 (CCH_3), 32.9 (d, $^1J_{C,P}$ = 138 Hz, PCH_2), 62.0 (OCH_2), 80.3 (CMe_3), 118.4 ($C_{aromatic}$), 125.5 ($C_{aromatic}$), 130.1 ($C_{aromatic}$), 137.4 ($C_{aromatic}$), 152.8-

dx.doi.org/10.1021/jm301435z | J. Med. Chem. 2013, 56, 1629−1640

($C_{aromatic}$). ESI-MS (m/z): measured 366.03 $[M + Na]^+$; expected 366.14

***tert*-Butyl (4-((Diethoxyphosphoryl)methyl)phenyl)(methyl)-carbamate (3).** To an oven-dried 100 mL round-bottom flask purged with argon and fitted with a magnetic stir bar was added sodium hydride (0.35 g, 8.74 mmol, 60% dispersion in mineral oil). The sodium hydride was washed three times with hexanes (6 mL), and the solvent was discarded. Compound **2** (2.0g, 5.82 mmol) was added under argon, and the mixture was suspended in dry THF (18 mL). The mixture was cooled to 0 °C, and methyl iodide (0.75 mL, 11.7 mmol, 2.28 g/mL) was added dropwise. The mixture was allowed to warm to room temperature and stirred under argon overnight. The reaction was quenched with water, and the THF was removed under vacuum. The residue was dissolved in EtOAc and water, and the aqueous layer was extracted three times with EtOAc. The organic layers were combined and washed twice with water and once with brine. The organic layer was dried over $MgSO_4$, filtered, and concentrated to give pure **3** as a yellow oil (1.96 g, 94%). ^{1}H NMR ($CDCl_3$, 400 MHz) δ: 1.23 (6H, t, J = 7.2 Hz, CH_2CH_3), 1.42 (9H, s, CCH_3), 3.11 (2H, d, $^3J_{H,P}$ = 21.6 Hz, PCH_2), 3.22 (3H, s, NCH_3), 3.94−4.07 (4H, m, OCH_2), 7.16 (2H, br d, J = 8.0 Hz, ArH), 7.24 (2H, m, ArH). ^{13}C NMR ($CDCl_3$, 100 MHz) δ: 16.3 (CH_2CH_3), 28.1 (CCH_3), 33.0 (d, $^2J_{C,P}$ = 138 Hz, PCH_2), 37.1 (NCH_3), 61.9 (OCH_2), 80.1 (CMe_3), 125.4 ($C_{aromatic}$), 128.4 ($C_{aromatic}$), 129.7 ($C_{aromatic}$), 142.4 ($C_{aromatic}$), 154.5 ($C_{aromatic}$). ESI-MS (m/z): measured 380.06 $[M + Na]^+$; expected 380.16

***(E)*-*tert*-Butyl Methyl(4-(4-(prop-2-yn-1-yloxy)styryl)phenyl)-carbamate (5).** A mixture of compound **3** (3, 1.12 g, 3.14 mmol) and sodium hydride (0.25 g, 6.29 mmol) in dry DMF (5 mL) was stirred under Ar for 1 h. A solution of 4-(prop-2-yn-1-yloxy)benzaldehyde (**4**, 0.40 g, 2.51 mmol) in dry DMF (2 mL) was added and the mixture stirred for an additional 12 h. The reaction mixture was diluted with EtOAc (50 mL) and extracted with $K_2CO_{3(aq)}$ 10% (2 × 30 mL). The organic layer was dried over sodium sulfate, filtered, and evaporated. The residue was purified by column chromatography over silica gel, eluting with DCM. The fractions containing the product were joined and evaporated under reduced pressure to give **5** (0.76 g, 83%) as a white solid. ^{1}H NMR ($CDCl_3$, 400 MHz) δ: 1.46 (9H, s, OCH_3), 2.54 (1H, t, J = 2.4 Hz, CCH), 3.27 (3H, s, NCH_3), 4.70 (2H, d, J = 2.4 Hz, OCH_2), 6.93−7.05 (4H, m, CH_{alkene} and ArH), 7.22 (2H, d, J = 8.4 Hz, ArH), 7.42−7.47 (4H, m, ArH). ^{13}C NMR ($CDCl_3$, 100 MHz) δ: 28.29 (OCH_3), 37.15 (NCH_3), 55.76 (OCH_2), 75.60 (CH_{alkyne}), 78.38 (C_{alkyne}), 80.32 ($OCMe_3$), 115.03 ($CH_{aromatic}$), 125.40 ($CH_{aromatic}$), 126.29 ($CH_{aromatic}$ + $C_{aromatic}$), 127.56 ($CH_{aromatic}$), 127.70 (CH_{alkene}), 130.90 (CH_{alkene}), 134.47 ($C_{aromatic}$), 142.77 ($C_{aromatic}$), 154.61 ($C_{aromatic}$), 157.06 (CO). ESI-MS (m/z): measured 364.33 $[M + H]^+$; expected 364.19

***(E)*-*tert*-Butyl (4-(4-((1-(3-aminopropyl)-1*H*-1,2,3-triazol-4-yl)methoxy)styryl)phenyl)methylcarbamate (6).** A suspension of **5** (0.62 g, 1.71 mmol), 3-azidopropan-1-amine (0.26 g, 2.57 mmol), Hunig's base (0.55 g, 4.28 mmol), and copper(I) iodide (0.049 g, 0.26 mmol) in dichloromethane (25 mL) was stirred under argon. After 3 h a fresh aliquot of 3-azidopropan-1-amine (0.21 g, 2.12 mmol) was added in a dichloromethane solution (2 mL). The mixture was stirred under Ar at room temperature for 12 h. The solvent was removed under reduced pressure, and the residue was dissolved in ethyl acetate (25 mL) and extracted with NH_4OH_{aq} 0.1 M (2 × 25 mL). The aqueous extracts were combined and washed with dichloromethane (2 × 25 mL). The dichloromethane solutions were combined and extracted with NH_4OH_{aq} 0.1 M (4 × 50 mL) and brine (1 × 50 mL). The organic layer was dried over sodium sulfate and filtered. The solvent was removed under reduced pressure, and the residue was purified by column chromatography over silica gel, eluting with a gradient of methanol in dichloromethane from 0% to 5%. The fractions containing the product were combined and evaporated to give **6** (0.43 g, 54%) as a white solid. ^{1}H NMR (400 MHz, $CDCl_3$) δ: 1.45 (9H, s, OCH_3), 2.02 (2H, q, J = 6.8 Hz, $CH_2CH_2CH_2$), 2.72 (2H, br, NH_2), 3.25 (3H, s, NCH_3), 4.47 (2H, t, J = 6.9 Hz, CH_2N), 5.21 (2H, s, OCH_2), 6.90−7.05 (4H, m, ArH and CH_{alkene}), 7.20 (2H, m, ArH), 7.42 (4H, m, ArH), 7.63 (1H, s, NCH). ^{13}C NMR ($CDCl_3$, 100 MHz) δ: 28.28 (OCH_3), 33.30 ($CH_2CH_2CH_2$), 37.15 (NCH_3), 38.48 (H_2NCH_2), 47.73 (NCH_2), 62.03 (OCH_2), 80.32 (CMe_3), 114.92 ($CH_{aromatic}$), 122.77 ($C_{aromatic\ triazol}$), 125.39 ($CH_{aromatic}$), 126.11 ($C_{aromatic}$), 126.26 ($CH_{aromatic}$), 127.62 ($CH_{aromatic}$), 127.71(CH_{alkene}), 130.55 (CH_{alkene}), 134.48 ($C_{aromatic}$), 142.74 ($C_{aromatic}$), 143.97 ($C_{aromatic\ triazol}$), 154.61 ($C_{aromatic}$), 157.78 (CO). ESI-MS (m/z): measured 464.07 $[M + H]^+$; expected 464.27

***(E)*-Tri-*tert*-butyl 2,2′,2″-(10-(2-((3-(4-((4-(4-((*tert*-Butoxycarbonyl)(methyl)amino)styryl)phenoxy)methyl)-1*H*-1,2,3-triazol-1-yl)propyl)amino)-2-oxoethyl)-1,4,7,10-tetraaza-cyclododecane-1,4,7-triyl)triacetate (8).** A solution of **7** (0.48 g, 0.83 mmol), **6** (0.35 g, 0.76 mmol), HBTU (0.30 g, 0.79 mmol), HOBT (0.12 g, 0.79 mmol), and DIPEA (0.15 g, 1.13 mmol) in dimethylformamide (7 mL) was stirred at room temperature for 12 h. The solution was diluted with EtOAc (25 mL) and extracted with water (3 × 25 mL). The organic layer was dried over Na_2SO_4, filtered, and evaporated under reduced pressure. The residue was purified by column chromatography on silica gel, eluting with a gradient of methanol in dichloromethane from 0% to 5%. The fractions containing pure product **8** were evaporated. The fractions containing the product contaminated with aromatic byproducts were combined and evaporated. The residue was dissolved in dichloromethane (30 mL) and extracted with CH_3COONa_{aq} 0.1 M (6 × 50 mL) and brine (1 × 50 mL). The organic phase was dried over Na_2SO_4, filtered, and evaporated under reduced pressure to give compound **8** as an amber glassy solid. The combined yield of product **8** was 92% (0.71 g). ^{1}H NMR (400 MHz, $CDCl_3$) δ: 1.28−1.51 (36H, m, br, CCH_3), 1.67−3.64 (28H, br, $CH_{2\ macrocycle}$, NCH_2), 3.23 (3H, s, NCH_3), 4.38 (2H, m, CH_2N), 5.17 (2H, s, OCH_2), 6.87−7.02 (4H, m, ArH and CH_{alkene}), 7.17 (2H, d, J = 8.4 Hz, ArH), 7.40 (4H, d, J = 8.6 Hz, ArH), 7.88 (1H, s, $CH_{triazol}$). ^{13}C NMR ($CDCl_3$, 100 MHz) δ: 27.72 ($OC(CH_3)_3$, br), 28.18 ($OC(CH_3)_3$), 29.89 ($CH_2CH_2CH_2$), 36.02 (H_2NCH_2), 37.06 (NCH_3), 47.61 (NCH_2), 47.1−53.5 ($NCH_{2\ ring}$, br), 55.2−55.7 ($NCH_{2\ acetic}$, br), 61.42 (OCH_2), 80.20 (CMe_3), 81.5−82.05 ($CMe_{3\ ester}$, br), 114.90 ($CH_{aromatic}$), 123.91 ($CH_{aromatic}$), 125.27 ($CH_{aromatic}$), 125.74 ($C_{aromatic}$), 126.14 ($CH_{aromatic}$), 127.49 ($CH_{aromatic}$), 127.76 (CH_{alkene}), 130.16 (CH_{alkene}), 134.45 ($C_{aromatic}$), 142.55 ($C_{aromatic}$), 143.14 ($C_{aromatic\ triazol}$), 154.53 ($C_{aromatic}$), 157.87 (NCO), 171.9−173.9 ($CO_{macrocycle}$).

***(E)*-2,2′,2″-(10-(2-((3-(4-((4-(4-(Methylamino)styryl)-phenoxy)methyl)-1*H*-1,2,3-triazol-1-yl)propyl)amino)-2-oxoethyl)-1,4,7,10-tetraazacyclododecane-1,4,7-triyl)triacetic Acid (9).** A solution of **8** (0.16 g, 0.16 mmol) in trifluoroacetic acid (2 mL) was stirred at room temperature for 24 h. Trifluoroacetic acid (TFA) was evaporated under reduced pressure. The residue was dissolved in a minimum amount of water and loaded on a Hypersep C18 SPE cartridge (1 g bed). The cartridge was eluted with a gradient of water/TFA (99.9:0.1, eluant A) and acetonitrile/TFA (99.9:0.1, eluant B). The cartridge was eluted extensively with solvent A and then with solvent A/solvent B 9/1 (15 mL). The product was recovered eluting with solvent A/solvent B 8/2. The fraction containing the product was evaporated to give **9**·xTFA (0.085 g) as an amber glass solid. ^{1}H NMR (400 MHz, pH ≈ 3, D_2O, external ref t-BuOH) δ: 1.96 (2H, q, J = 6.6 Hz $CH_2CH_2CH_2$), 2.70−4.44 (26H, br m, $CH_{2\ macrocycle}$, NCH_2), 2.91 (3H, s, NCH_3), 4.32 (2H, t, J = 6.5 Hz, CH_2N), 4.95 (2H, s, OCH_2), 6.57 (1H, d, J = 16.1 Hz, CH_{alkene}), 6.68−6.78 (3H, m, ArH, CH_{alkene}), 7.15 (2H, d, J = 8.7 Hz, ArH), 7.23 (4H, s, ArH) 7.94 (1H, s, $CH_{triazol}$); ^{13}C NMR (600 MHz, 50 C, pH ≈ 3, D_2O, external ref t-BuOH) δ: 30.68 ($CH_2CH_2CH_2$), 38.34 (NCH_2), 38.78 (NCH_2), 40.93 (NCH_2), 50.03 ($NCH_{2\ ring}$, br), 51.04 ($NCH_{2\ ring}$, br), 52.5 ($NCH_{2\ ring}$, br), 55.34 ($NCH_{2\ acetic}$, br), 56.05 ($NCH_{2\ acetic}$, br), 56.66 ($NCH_{2\ acetic}$, br), 63.03 (OCH_2), 117.40 ($CH_{aromatic}$), 118.24 (q, J = 292 Hz, CF_3) 124.00 ($CH_{aromatic}$), 126.94 ($C_{aromatic}$), 127.01 ($CH_{aromatic}$), 129.57 (CH_{alkene}), 130.02 (CH_{alkene}), 131.63 ($CH_{aromatic}$), 132.19 ($CH_{aromatic}$), 136.78 ($C_{aromatic}$), 140.6 ($C_{aromatic}$), 144.98 ($C_{aromatic\ triazol}$), 159.4 ($C_{aromatic}$), 164.29 (q, J = 35.3 Hz, CF_3COOH), 173.84 (very br, CO). ESI-MS (m/z): measured 750.32 $[M + H]^+$; expected 750.39

Gadolinium (*E*)-2,2′,2″-(10-(2-((3-(4-((4-(4-(Methylamino)-styryl)phenoxy)methyl)-1*H*-1,2,3-triazol-1-yl)propyl)amino)-2-oxoethyl)-1,4,7,10-tetraazacyclododecane-1,4,7-triyl)triacetic

dx.doi.org/10.1021/jm301435z | J. Med. Chem. 2013, 56, 1629−1640

Acetate (10). The pH of a solution of **9**·*x*TFA (0.019 g) in deionized water (10 mL) was adjusted to 5 with $NaOH_{aq}$ 1 M. A solution of $GdCl_3$ (6.09 mg, 0.023 mmol) in water (4.0 mL) was added in four aliquots, maintaining the pH between 5.5 and 6 with $NaOH_{aq}$ 1 M. The solution was stirred at room temperature for 5 h, and subsequently the temperature was raised to 60 C and the reaction continued for 12 h. The solution was allowed to cool to room temperature, and the pH was adjusted to 9.5 with $NaOH_{aq}$ 1 M. The solution was then filtered through a 0.2 μm syringe filter and immediately loaded onto a Hypersep C18 SPE cartridge (1 g bed). The cartridge was eluted with a gradient of water and acetonitrile from water/acetonitrile 100/0 to water/acetonitrile 60/40. The fractions containing the product were concentrated under reduced pressure to remove the organic solvent and then lyophilized to give **10** (0.017g, 50% over two steps) as a yellow solid. ESI-MS (*m*/*z*): measured 905.2 $[M + H]^+$; expected 905.29. A correct isotopic pattern was observed. Elemental analysis calcd (%) for $C_{37}H_{48}N_9O_8Gd·3H_2O$: C 46.68, H 5.64, N 13.24. Found: C 46.76, H 5.54, N 12.93.

Animals. All animal experiments were performed in accordance with guidelines approved by the Institutional Animal Care and Use Committee of Case Western Reserve University (Protocols 2010-0006, 2010-0007). Two-month-old Swiss-Webster R/J mice were purchased from Harlan Laboratories, Indianapolis, IN. Two-month-old C57BL/6 mice were obtained from The Jackson Laboratory, Bar Harbor, ME. Sprague−Dawley rats were purchased from Harlan Laboratories, Haslett, MI. The *Plp*-Akt-DD transgenic mice were generated as described previously and used at 2 months of age.[32,33] Briefly, the transgenic mice expressing constitutively active Akt (HAAkt308D473D, Akt-DD) driven by the *Plp* promoter were generated and used as a hypermyelinated animal model. The Akt cDNA was inserted into the AscI/PacI sites of the modified *Plp* promoter cassette, and hypermyelination was induced after the *Plp* promoter/Akt-DD insert was injected into SJL/SWR F1 mice. Positive founders were identified by PCR amplification of tail DNA using IntronSV40F (5′-GCAGTGGACCACGGTCAT-3′) and Akt lower (5′-CTGGCAACTAGAAGGCACAG-3′) primer pairs. Analyses were done from wild-type littermate mice in all developmental experiments and, when possible, with older animals.

Induction of LPC Lesions. One Sprague−Dawley rat was anesthetized by ip injection of 225 μL of rodent cocktail [9 parts ketamine (100 mg/mL) + 9 parts xylazine (20 mg/mL) + 3 parts acepromazine (10 mg/mL) + 79 parts sterile saline]. The skull was shaved, and a 3 cm longitudinal incision was made on the scalp. A burr hole was created using a spherical dental burr over the site of the intended injection. Then 6 μL of a 1% LPC solution was injected at a rate 0.25 μL/min. The injection coordinates were AP = 0.0 mm, ML = 2.0 mm, DV = 3.2 mm, corresponding to the corpus callosum. After the injection the incision was sutured and the animal allowed to recover while being warmed with a heating pad. The lesions were allowed to develop for 7 days and subsequently the animal brain was used to prepare frozen sections as described below.

Preparation of Frozen Sections. Mice were deeply anesthetized with isoflurane and perfused via the ascending aorta with PBS followed by 4% paraformaldehyde in PBS. Brains were removed and incubated for 24 h in 4% paraformaldehyde at 4 °C, and then the tissues were incubated in 30% sucrose at 4 °C until submerged. Frozen sections were used for fluorescence microscopy. For preparation of fresh frozen sections, the cryoprotected tissues were first frozen in OCT on dry ice before axial sectioning (20 μm) with a cryostat at −20 °C. Tissue sections from the midline of the brain containing the whole corpus callosum were selected for staining. Stained sections were covered with fluorescence mounting medium (Vectashield, Vector Laboratories) and stored at 4 °C for future analysis.

Chemical Staining. Freshly frozen sections 20 μm in thickness were incubated in 0.1% Triton-100 in 1× PBS for 10 min and then incubated in a solution of **10** (100 μM) in H_2O for 30 min at room temperature. The fresh frozen sections were then washed three times for 5 min each with PBS before coverslipping with fluorescence mounting medium. Images of the stained mouse brain sections were acquired on a Nikon TE2000 inverted microscope (UV-2E/C Ex, 340−380; DM, 400; BA, 435−485) or with a Leica DM5000B microscope equipped with an HCX PL FLUOTAR 1.25×/0.04 objective and using the A4 filter (360/40 nm band-pass excitation, 400 nm dichromatic mirror, 470/40 nm band-pass suppression).

Intracerebroventricular Injection of Gd Complexes. Sprague−Dawley rats were anesthetized by ip injection of 200−250 μL of rodent cocktail (9 parts ketamine (100 mg/mL) + 9 parts xylazine (20 mg/mL) + 3 parts acepromazine (10 mg/mL) + 79 parts sterile saline) and were fixed to the rat head-restraining stereotaxic surgical table. The skull was shaved and a 3 cm longitudinal incision was made on the scalp. A burr hole was created using a spherical dental burr over the site of the intended injection. A water solution of **10** or compound **11** (7 mM, 10 μL, 70 nmol) was injected into the brain through a 10 μL syringe equipped with a 28 gauge needle. After injection the incision was sutured and the animals allowed to recover consciousness while warmed with a heating pad. The injections were performed on both sides of the brain in the lateral ventricles with half of the dose injected on each side. Typical coordinates for the injection sites relative to the bregma are AP = −0.5 ± 0.1 mm, ML = 2.3 ± 0.1 mm, DV = 3.5 ± 0.1 mm.

In Situ Staining of Myelin. The rats that were used for MR imaging were euthanized less than 48 h after compound **10** intracerebroventricular infusion and perfused to remove the blood, and the brains were extracted and sectioned to prepare frozen axial sections. Images of the stained mouse brain sections were acquired on a Nikon TE2000 inverted microscope (UV-2E/C Ex, 340−380; DM, 400; BA, 435−485).

Relaxometry. The relaxivity of **10** was measured at 1.41 T (40 °C) and 0.47 T (40 °C) on a Bruker minispec and at 9.4 T (21 °C) on a Varian Inova 400 NMR system equipped with a 5 mm broadband probe. The longitudinal relaxation rates of five water solutions, with concentrations of compound **10** ranging from 0 to 0.7 mM, were measured using an inversion recovery pulse sequence with at least 10 inversion times. Attention was paid to ensure that the relaxation delay between pulses was at least $5T_1$. The absence of free Gd(III) was confirmed using a standard colorimetric test with xylenol orange.

MR Imaging. All MR experiments were performed at 9.4 T (Bruker "BIOSPEC", Bruker, Germany) using a 60 mm diameter volume coil. Anesthesia was maintained by mask inhalation of isoflurane vaporized at concentrations of up to 4% in the induction phase, at 1.5% during the imaging experiments. Prior to measurement of the longitudinal relaxation time, axial images of the rat brain were acquired, using a multislice RARE pulse sequence (TE = 11.3 ms, TR = 5000 ms, spatial resolution = 0.195 × 0.195 mm/pixel, matrix size 256 × 256, 30 slices, slice thickness = 0.5 mm, 1 average), for the identification of the region of interest (ROI). T_1 measurements were carried out using a spin−echo multiple TR saturation recovery method with at least 10 TRs (TE = 6.99 ms, TR = 385−12500 ms, spatial resolution = 0.195 × 0.195 mm/pixel, matrix size = 256 × 256, 30 slices, slice thickness = 0.5 mm, 1 average). T_1 maps were generated using the QuickVol II plug-in in ImageJ. The animals were imaged twice using a spin−echo multiple TR saturation recovery method 5−7 h after injection and then again 20−24 h after injection.

■ ASSOCIATED CONTENT

Supporting Information

Fluorimetric characterization of compound **10** and synthesis and characterization of compound **11**. This material is available free of charge via the Internet at http://pubs.acs.org.

■ AUTHOR INFORMATION

Corresponding Author

*Telephone: (216) 844-3288. Fax: (216) 844-8062. E-mail: yanming.wang@case.edu.

Notes

The authors declare no competing financial interest.

■ ACKNOWLEDGMENTS

We gratefully acknowledge financial support through grants from the Department of Defense (Grant W81XWH-10-1-0842), National Multiple Sclerosis Society (Grant RG 4339-A-2), and NIH/NINDS (Grant R01 NS061837).

■ ABBREVIATIONS USED

DIPEA, *N*,*N*-diisopropylethylamine; DMF, dimethylformamide; DOTA, tetraazacyclododecanetetraacetic acid; DTPA, diethylenetriamine pentaacetic acid; Gd-DODAS, gadolinium (*E*)-2,2′,2″-(10-(2-((3-(4-((4-(4-(methylamino)styryl)-phenoxy)methyl)-1*H*-1,2,3-triazol-1-yl)propyl)amino)-2-oxoethyl)-1,4,7,10-tetraazacyclododecane-1,4,7-triyl)triacetic acetate; HBTU, *O*-(benzotriazol-1-yl)-*N*,*N*,*N*′,*N*′-tetramethyluronium hexafluorophosphate; HOBT, 1-hydroxybenzotriazole; MBP, myelin basic protein; MIC, gadolinium(III) [4,10-bis-carboxymethyl-7-({3-[3-(4-dimethylaminophenyl)-2-oxo-2*H*-chromen-7-yloxy]propylcarbamoyl}methyl)-1,4,7,10-tetraazacyclododec-1-yl]acetate; PET, positron emission tomography; TFA, trifluoroacetic acid; THF, tetrahydrofuran

■ REFERENCES

(1) Quarles, R. H.; MacKlin, W. B.; Morell, P. Myelin Formation, Structure and Biochemistry. In *Basic Neurochemistry: Molecular, Cellular, and Medical Aspects*; Siegel, G. J., Albers, R. W., Brady, S., Price, D., Eds.; Elsevier Academic: Burlington, MA, 2006; pp 51−72.

(2) Nave, K.-A. Myelination and support of axonal integrity by glia. *Nature* **2010**, *468*, 244−252.

(3) Trapp, B. D.; Nave, K. A. Multiple sclerosis: an immune or neurodegenerative disorder? *Annu. Rev. Neurosci.* **2008**, *31*, 247−269.

(4) Hauw, J. J.; Delaere, P.; Seilhean, D.; Cornu, P. Morphology of demyelination in the human central nervous system. *J. Neuroimmunol.* **1992**, *40*, 139−152.

(5) Pugliatti, M.; Sotgiu, S.; Rosati, G. The worldwide prevalence of multiple sclerosis. *Clin. Neurol. Neurosurg.* **2002**, *104*, 182−191.

(6) Ascherio, A.; Munger, K. L.; Luenemann, J. D. The initiation and prevention of multiple sclerosis. *Nat. Rev. Neurol.* **2012**, *8*, 602−612.

(7) Lassmann, H.; van Horssen, J.; Mahad, D. Progressive multiple sclerosis: pathology and pathogenesis. *Nat. Rev. Neurol.* **2012**, *8*, 647−656.

(8) Krumbholz, M.; Derfuss, T.; Hohlfeld, R.; Meinl, E. B cells and antibodies in multiple sclerosis pathogenesis and therapy. *Nat. Rev. Neurol.* **2012**, *8*, 613−623.

(9) Deraos, G.; Chatzantoni, K.; Matsoukas, M.-T.; Tselios, T.; Deraos, S.; Katsara, M.; Papathanasopoulos, P.; Vynios, D.; Apostolopoulos, V.; Mouzaki, A.; Matsoukas, J. Citrullination of linear and cyclic altered peptide ligands from myelin basic protein (MBP87-99) epitope elicits a Th1 polarized response by T cells isolated from multiple sclerosis patients: implications in triggering disease. *J. Med. Chem.* **2008**, *51*, 7834−7842.

(10) Ioannou, M.; Alissafi, T.; Lazaridis, I.; Deraos, G.; Matsoukas, J.; Gravanis, A.; Mastorodemos, V.; Plaitakis, A.; Sharpe, A.; Boumpas, D.; Verginis, P. Crucial role of granulocytic myeloid-derived suppressor cells in the regulation of central nervous system autoimmune disease. *J. Immunol.* **2012**, *188*, 1136−1146.

(11) Nagulapalli, M.; Parigi, G.; Yuan, J.; Gsponer, J.; Deraos, G.; Bamm, V. V.; Harauz, G.; Matsoukas, J.; de Planque, M. R. R.; Gerothanassis, I. P.; Babu, M. M.; Luchinat, C.; Tzakos, A. G. Recognition pliability is coupled to structural heterogeneity: a calmodulin intrinsically disordered binding region complex. *Structure* **2012**, *20*, 522−533.

(12) Lövblad, K.-O.; Anzalone, N.; Dörfler, A.; Essig, M.; Hurwitz, B.; Kappos, L.; Lee, S.-K.; Filippi, M. MR imaging in multiple sclerosis: review and recommendations for current practice. *Am. J. Neuroradiol.* **2010**, *31*, 983−989.

(13) Polman, C. H.; Reingold, S. C.; Banwell, B.; Clanet, M.; Cohen, J. A.; Filippi, M.; Fujihara, K.; Havrdova, E.; Hutchinson, M.; Kappos, L.; Lublin, F. D.; Montalban, X.; O'Connor, P.; Sandberg-Wollheim, M.; Thompson, A. J.; Waubant, E.; Weinshenker, B.; Wolinsky, J. S. Diagnostic criteria for multiple sclerosis: 2010 revisions to the McDonald criteria. *Ann. Neurol.* **2011**, *69*, 292−302.

(14) Graham-Rowe, D. Drugs: an injection of hope. *Nature* **2012**, *484*, S4−S4.

(15) Zivadinov, R.; Bakshi, R. Role of Magnetic Resonance Imaging in the Diagnosis and Prognosis of Multiple Sclerosis. In *Multiple Sclerosis: Etiology, Diagnosis, and New Treatment Strategies*; Humana Press Inc: Totowa, NJ, 2005; pp 55−89.

(16) Bakshi, R.; Thompson, A. J.; Rocca, M. A.; Pelletier, D.; Dousset, V.; Barkhof, F.; Inglese, M.; Guttmann, C. R.; Horsfield, M. A.; Filippi, M. MRI in multiple sclerosis: current status and future prospects. *Lancet Neurol.* **2008**, *7*, 615−625.

(17) Bendszus, M.; Ladewig, G.; Jestaedt, L.; Misselwitz, B.; Solymosi, L.; Toyka, K.; Stoll, G. Gadofluorine M enhancement allows more sensitive detection of inflammatory CNS lesions than T2-w imaging: a quantitative MRI study. *Brain* **2008**, *131*, 2341−2352.

(18) Wessig, C. Detection of blood−nerve barrier permeability by magnetic resonance imaging. *Methods Mol. Biol.* **2011**, *686*, 267−271.

(19) Wu, C.; Tian, D.; Feng, Y.; Polak, P.; Wei, J.; Sharp, A.; Stankoff, B.; Lubetzki, C.; Zalc, B.; Mufson, E. J.; Gould, R. M.; Feinstein, D. L.; Wang, Y. A novel fluorescent probe that is brain permeable and selectively binds to myelin. *J. Histochem. Cytochem.* **2006**, *54*, 997−1004.

(20) Wu, C.; Wei, J.; Tian, D.; Feng, Y.; Miller, R. H.; Wang, Y. Molecular probes for imaging myelinated white matter in CNS. *J. Med. Chem.* **2008**, *51*, 6682−6688.

(21) Wang, Y.; Wu, C.; Caprariello, A. V.; Somoza, E.; Zhu, W.; Wang, C.; Miller, R. H. In vivo quantification of myelin changes in the vertebrate nervous system. *J. Neurosci.* **2009**, *29*, 14663−14669.

(22) Wang, C.; Popescu, D. C.; Wu, C.; Zhu, J.; Macklin, W.; Wang, Y. In situ fluorescence imaging of myelination. *J. Histochem. Cytochem.* **2010**, *58*, 611−621.

(23) Wu, C.; Wang, C.; Popescu, D. C.; Zhu, W.; Somoza, E. A.; Zhu, J.; Condie, A. G.; Flask, C. A.; Miller, R. H.; Macklin, W.; Wang, Y. A novel PET marker for in vivo quantification of myelination. *Bioorg. Med. Chem.* **2010**, *18*, 8592−8599.

(24) Wang, C.; Wu, C.; Popescu, D. C.; Zhu, J.; Macklin, W. B.; Miller, R. H.; Wang, Y. Longitudinal near-infrared imaging of myelination. *J. Neurosci.* **2011**, *31*, 2382−2390.

(25) Wang, C.; Wu, C.; Zhu, J.; Miller, R. H.; Wang, Y. Design, synthesis, and evaluation of coumarin-based molecular probes for imaging of myelination. *J. Med. Chem.* **2011**, *54*, 2331−2340.

(26) Frullano, L.; Wang, C.; Miller, R. H.; Wang, Y. A myelin-specific contrast agent for magnetic resonance imaging of myelination. *J. Am. Chem. Soc.* **2011**, *133*, 1611−1613.

(27) Frullano, L.; Zhu, J.; Wang, C.; Wu, C.; Miller, R. H.; Wang, Y. Myelin imaging compound (MIC) enhanced magnetic resonance imaging of myelination. *J. Med. Chem.* **2012**, *55*, 94−105.

(28) Yang, J.-S.; Chiou, S.-Y.; Liau, K.-L. Fluorescence enhancement of *trans*-4-aminostilbene by *N*-phenyl substitutions: the "amino conjugation effect". *J. Am. Chem. Soc.* **2002**, *124*, 2518−2527.

(29) Schmued, L.; Bowyer, J.; Cozart, M.; Heard, D.; Binienda, Z.; Paule, M. Introducing Black-Gold II, a highly soluble gold phosphate complex with several unique advantages for the histochemical localization of myelin. *Brain Res.* **2008**, *1229*, 210−217.

(30) Franklin, K. B. J.; Paxinos, G. *The Mouse Brain in Stereotaxic Coordinates*, 3rd ed.; Elsevier Academic Press Inc.: San Diego, CA, 2007.

(31) Paxinos, G.; Watson, C. *The Rat Brain in Stereotaxic Coordinates*, 6th ed.; Elsevier Academic Press Inc.: San Diego, CA, 2007.

(32) Flores, A. I.; Narayanan, S. P.; Morse, E. N.; Shick, H. E.; Yin, X.; Kidd, G.; Avila, R. L.; Kirschner, D. A.; Macklin, W. B. Constitutively active Akt induces enhanced myelination in the CNS. *J. Neurosci.* **2008**, *28*, 7174−7183.

(33) Narayanan, S. P.; Flores, A. I.; Wang, F.; Macklin, W. B. Akt signals through the mammalian target of rapamycin pathway to regulate CNS myelination. *J. Neurosci.* **2009**, *29*, 6860−6870.
(34) Rohrer, M.; Bauer, H.; Mintorovitch, J.; Requardt, M.; Weinmann, H.-J. Comparison of magnetic properties of MRI contrast media solutions at different magnetic field strengths. *Invest. Radiol.* **2005**, *40*, 715−724.
(35) de Sousa Paulo, L.; Livramento Joao, B.; Helm, L.; Merbach Andre, E.; Meme, W.; Doan, B.-T.; Beloeil, J.-C.; Prata Maria, I. M.; Santos Ana, C.; Geraldes Carlos, F. G. C.; Toth, E. In vivo MRI assessment of a novel GdIII-based contrast agent designed for high magnetic field applications. *Contrast Media Mol. Imaging* **2008**, *3*, 78−85.
(36) Caravan, P.; Farrar, C. T.; Frullano, L.; Uppal, R. Influence of molecular parameters and increasing magnetic field strength on relaxivity of gadolinium- and manganese-based T1 contrast agents. *Contrast Media Mol. Imaging* **2009**, *4*, 89−100.